Electrochimica Acta 283 (2018) 1600–1608

Contents lists available at ScienceDirect

Electrochimica Acta

journal homepage: www.elsevier.com/locate/electacta

The role of internal cathodic support during the crevice corrosion of Ni-Cr-Mo alloys

J.D. Henderson [a], N. Ebrahimi [a], V. Dehnavi [a], M. Guo [a], D.W. Shoesmith [a, b], J.J. Noël [a, b, *]

[a] Department of Chemistry, The University of Western Ontario, London, ON, N6A 5B7, Canada
[b] Surface Science Western, The University of Western Ontario, London, ON, N6G 0J3, Canada

ARTICLE INFO

Article history:
Received 9 February 2018
Received in revised form
30 June 2018
Accepted 10 July 2018
Available online 11 July 2018

Keywords:
Ni-Cr-Mo alloys
Crevice corrosion
Proton reduction
Localized corrosion

ABSTRACT

Coupling of metal oxidation in crevice corrosion to both O_2 reduction on surfaces external to the crevice and H^+ reduction occurring within the crevice, was studied using a galvanostatic crevice corrosion technique in conjunction with weight loss analyses. Results suggest internal H^+ reduction is a significant contributor to the crevice corrosion of the studied alloys in 5 M NaCl at 120 °C. Repeat experiments suggest damage can be as much as doubled by H^+ reduction. This process, however, can be minimized by alloying additions of Mo, which permit the deposition of Mo-rich corrosion products within an active crevice. Due to difficulties experienced during corrosion product removal, the results presented herein are anticipated to be underestimates of the actual extent of this process. Consequently, damage predictions based on the availability of O_2 and other oxidants in the service environment may significantly underestimate the actual extent of corrosion on Ni-Cr-Mo alloys.

1. Introduction

Ni-based alloys are industrially important due to their robust corrosion resistant properties. Typically containing measurable amounts of Cr and Mo, these alloys have found applications in a range of industries, including petrochemical, nuclear, and chemical processing. Understanding and predicting their corrosion performance, and designing new, optimized alloys, requires a fuller understanding of the role of alloying elements and the nature of the corrosion processes.

Alloying additions of Cr are understood to induce strongly passive behaviour, due to the growth of a Cr(III)-rich oxide layer, a feature similar to what is seen in stainless steels [1]. However, alloying elements are much more soluble in the face-centred cubic (FCC) crystal structure of Ni-alloys than they are in Fe-based alloys, which allows for the accommodation of greater amounts of alloying additions in Ni-based alloys, while avoiding the formation of possibly deleterious secondary phases.

Mo is typically added to increase the stability of the oxide film and resistance to localized corrosion processes [1,2]. Mo is also understood to supress active dissolution under conditions where Cr becomes soluble, including acidic and highly oxidizing environments [3]. However, the content of alloying elements must be adjusted carefully because they affect not only corrosion properties but also materials cost, mechanical performance, weldability, etc. Many attempts to suggest an optimal alloy composition have been made; however, such a composition has not yet been achieved.

According to critical crevice solution (CCS) theory, the initiation of active crevice corrosion involves the development of a deaerated, acidic solution within the occluded geometry [4,5]. Typically, crevice corrosion on Ni-based alloys is thought to be supported by O_2 reduction external to the occluded region. However, in the case of Ti-alloys, crevice corrosion has been shown to involve the coupling of metal dissolution to both O_2 reduction on external surfaces and H^+ reduction within the acidified crevice, as depicted in Fig. 1 [6]. The presence of this coupling has been shown to intensify damage by 400% or more on these alloys [6,7,8].

Recently, electrochemical evidence has suggested that cathodic support for crevice corrosion of Ni alloys can also involve both O_2 reduction outside the crevice and H^+ reduction in its interior, resulting in intensified damage on Ni-based alloys [9]. This was inferred from observations that more than the expected quantity of damage was incurred by coupons that were made to undergo crevice corrosion under the application of constant anodic current. Although initially presented as a possibility, this inference was later supported by findings that revealed that once initiated, crevice

* Corresponding author. Department of Chemistry, The University of Western Ontario, London, ON, N6A 5B7, Canada.
E-mail address: jjnoel@uwo.ca (J.J. Noël).

https://doi.org/10.1016/j.electacta.2018.07.048
0013-4686/

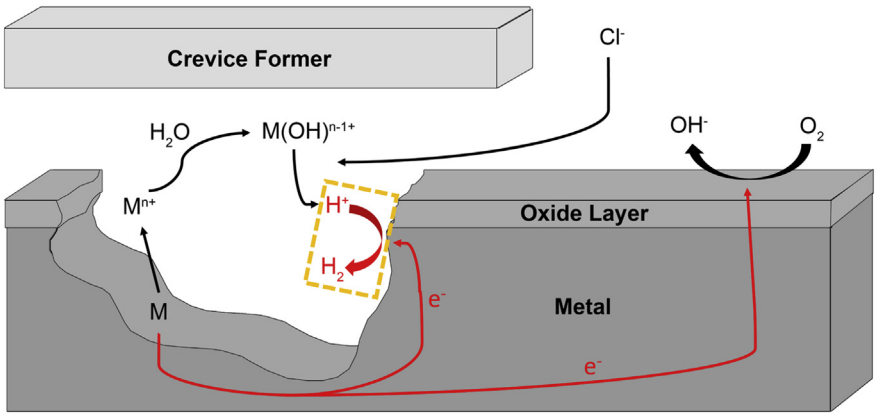

Fig. 1. Schematic representation of the critical crevice chemistry that develops within an active crevice [6].

corrosion on Ni-Cr-Mo alloys can support itself through an internal cathodic reaction [10]. It is no surprise that this feature has been overlooked in the literature, since many studies have focused on techniques such as potentiodynamic-galvanostatic-potentiodynamic (PD-GS-PD) tests. Although these techniques are effective in ranking the relative corrosion resistance of alloys in terms of breakdown/repassivation potentials, they provide no mechanistic information. The work presented herein was undertaken to more fully document this previously unexplored feature.

In this paper the presence of the previously overlooked internal cathodic reaction on Ni-based alloys is examined using a galvanostatic technique in conjunction with weight loss analyses. Repeat experiments suggest that propagation damage can be as much as doubled by the internal H^+ reduction reaction. Through the analysis of a series of commercial alloys with differing amounts of the same alloying elements, we are trying to understand how alloy composition affects this process. The Ni-based alloys Hastelloy G-30, C-22, and BC-1, were selected for this study, based mainly on their varying Mo-content, since Mo-rich corrosion products have been extensively studied and are believed to stifle active corrosion [11,12]. Herein, we evaluate the prevalence of the H^+ reduction reaction occurring during the crevice corrosion of Ni-based alloys in relation to the resulting damage morphology and the extent and type of corrosion product deposition.

2. Experimental

2.1. Material preparation

Alloy samples, provided by Haynes International (Kokomo, IN, USA), were received as mill-annealed sheets with a thickness of 3.18 mm (1/8″). Crevice coupons were formed from 15 mm wide strips cut from the plate stock. The compositions, as reported by Haynes International, are listed in Table 1.

Prior to electrochemical measurements, all coupons were ground using wet silicon carbide (SiC) paper, sequentially from P600 to P1200 grit, carefully sonicated in a 1:1 mixture of Type-1 water (Thermo Scientific Barnstead™ Nanopure™) and ethanol for 2 min, rinsed with Type-1 water, and then dried in a stream of argon gas. Polished crevice coupons were then stored in a vacuum desiccator for a 24-h period prior to use, to help assure an accurate gravimetric measurement.

Samples being prepared for electron backscatter diffraction were subjected to further polishing (1 μm diamond suspension) and a final etching step to expose grain boundaries. Different etching procedures were used for the various alloys due to differences in their corrosion resistance. Hastelloy G-30 was etched by manual swabbing with a mixture (3:2:2) of HCl, CH_3COOH, and HNO_3. Hastelloy C-22 and BC-1 were electrochemically etched in an oxalic acid solution (10 wt %) by the application of a 0.2 A cm^{-2} anodic current for 15 s.

Solutions of 5 M NaCl were prepared using reagent grade NaCl (Caledon Laboratory Chemicals, Georgetown, ON) and Type-1 water. Solutions were saturated with air by vigorous physical agitation immediately preceding each experiment.

2.2. Electrochemical setup

Crevice corrosion experiments were performed in a Hastelloy pressure vessel (Parr Instrument Co., Model 4621), outfitted as an electrochemical cell with four pressure-tight electrode feedthrough (Fig. 2). The interior of the vessel was lined with a polytetrafluoroethylene (PTFE) insert to prevent electrical contact of electrodes and electrolyte solution with the vessel walls and to protect the vessel from corrosion. All potential measurements were made using a homemade saturated Ag/AgCl (0.197 V vs SHE) reference electrode (RE). Prior to each experiment, the RE potential was measured against a 'master' saturated calomel electrode used only for the purpose of calibration. The counter electrode (CE) and all electrode leads were fabricated using the same material as the working electrode (WE) being studied to avoid galvanic coupling.

The WE was assembled using a single-crevice approach which has been extensively detailed elsewhere [13–15]. This design forms a single crevice between the V-shaped WE and a PTFE crevice

Table 1
Nominal compositions in weight % of studied alloys as reported by Haynes International. * indicates alloying element which constitutes the balance. M indicates an alloying element's maximum weight percentage.

Alloy	Ni	Cr	Mo	Fe	W	Cu	Nb	Co	Mn	V	Al	Si	C
G-30®	43*	30	5.5	15	2.5	2	0.8	5 M	1.5 M	0	0	0.8 M	0.03 M
C-22®	56*	22	13	3	3	0.5 M	0	2.5 M	0.5 M	0.35 M	0	0.08 M	0.01 M
BC-1®	62*	15	22	2 M	0	0	0	1 M	0.25	0	0.5 M	0.08 M	0.01 M

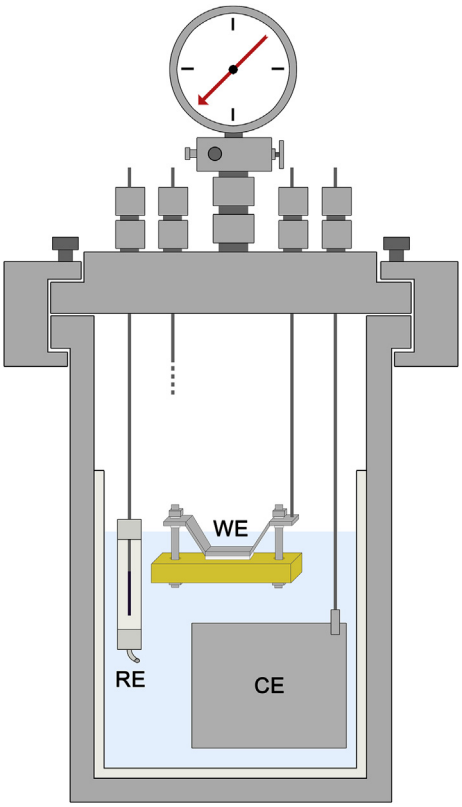

Fig. 2. Hastelloy pressure vessel outfitted as a 3-electrode electrochemical cell.

former, which are held securely by a Udel block. Udel bushings were used to prevent electrical contact between the WE and the rods and bolts used to secure the crevice assembly. This arrangement ensures the formation of a single electrically connected crevice.

Once assembled, the vessel was pressurized (~414 kPa) with ultra-high purity (UHP) nitrogen gas (Praxair, Mississauga, ON) and tested for leaks. The vessel was then placed in a heating mantle and the temperature was elevated to $120 \pm 2\,^{\circ}C$ and maintained there for the duration of the experiment. After the experimental temperature was established, crevice corrosion was initiated using galvanostatic polarization. The total applied charge (Q_A) was controlled by applying a constant current through the WE and manipulating the duration of an experiment. At applied currents of 100, 75, 50, and 25 μA, the corresponding experimental times were 1, 1.33, 2, and 4×10^6 s, respectively, in order to maintain a consistent QA of 100 C. Each experiment was monitored by measuring the potential response using a Solartron model 1284 potentiostat (Solartron Analytical, Hampshire, UK).

2.3. Surface analysis

Following electrochemical experiments, routine surface analysis was conducted using Hitachi S-4500 field emission and Hitachi SU3500 Variable Pressure scanning electron microscopes (SEM). Unless otherwise stated, corrosion products were removed prior to surface analysis, through a cleaning process involving both sonication and manual swabbing with cotton-tipped applicator sticks. Energy dispersive X-ray spectroscopy (EDX) was conducted on a Hitachi SU3500 Variable Pressure SEM in combination with an Oxford Aztec X-Max50 X-ray analyzer. Aztec software allowed for both point analyses as well as the acquisition of EDX maps.

Electron backscatter diffraction (EBSD) was conducted on a Hitachi SU6600 field emission gun scanning electron microscope (FEG-SEM). The FEG-SEM was outfitted with a HKL Nordly EBSD detector to collect Kikuchi patterns. Data analysis was carried out using the HKL Channel 5 software suite (Oxford Instruments). All crystal orientation information was indexed according to the FCC crystal structure.

Surface profilometry was conducted on a KLA Tencor P-10 Surface Profiler (Milpitas, CA, USA) and used to determine the maximum depth of penetration and overall damage morphology within a corroded crevice. The instrument was outfitted with a stylus containing a tungsten point, fixed with a diamond tip (radius ~2 μm). The stylus was scanned over the surface at 50 μm/s.

3. Results and discussion

3.1. Galvanostatic crevice corrosion

Detailed in Fig. 3 is the typical potential response of an artificial crevice while under galvanostatic control. Following the application of constant current, the potential increases rapidly due to oxide growth. The potential increase eventually reaches an approximately steady state in which the rates of film growth and destruction are approximately equal. It is in this region where passive oxide film breakdown attempts occur, resulting in negative-going potential transients. Typically, a large number of these transients are observed as the passive film breaks and the potential drops but then readily returns to the steady-state potential, i.e., the surface repassivates. However, over time, as the CCS chemistry develops as a result of chemical reactions during these metastable events within the occluded region, the likelihood that a given breakdown event will successfully initiate crevice corrosion increases. The success of any individual breakdown event in initiating crevice corrosion depends on the accumulation of incremental chemical changes resulting from prior initiation attempts. The total time required for a successful breakdown event is often referred to as the incubation time. Since features such as the incubation time rely heavily on the dynamic chemistry evolving within the crevice, only general observations are made. The overall behaviour has been discussed in previous publications which have utilized galvanostatic polarization to control the crevice corrosion of Ni-Cr-Mo alloys [9,10,13].

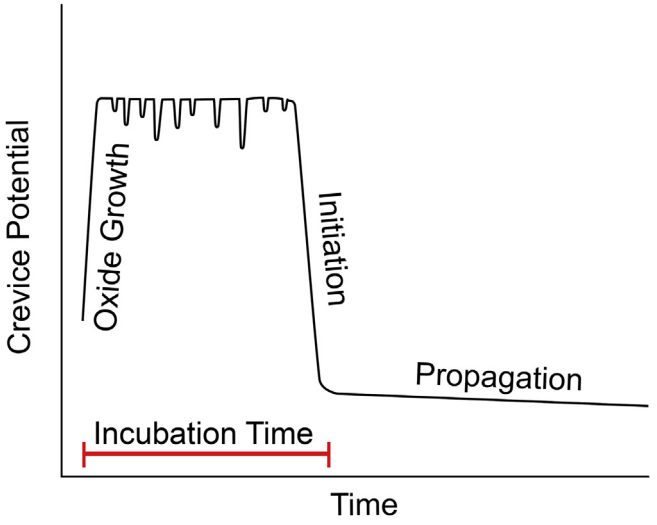

Fig. 3. Graphical representation of typical potential behaviour for a crevice electrode under galvanostatic control.

3.2. Potential behaviour of C-22

The typical response of alloy C-22 follows the behaviour described in Fig. 3, and is illustrated in Fig. 4 at applied currents of 100, 75, 50, and 25 μA. Initially, oxide growth occurs at approximately the same rate in each case, and is independent of the applied current. The maximum potential reached was however typically found to be higher with higher applied currents. A possible explanation for this is related to the nature of the film formed under varied applied currents. Jakupi et al. demonstrated that oxides grown at high applied potentials (>300 mV vs sat'd Ag/AgCl) were typically thick and defect-rich [13]. Although not explicitly demonstrated here, it is expected that higher applied currents result in similar thick, defect-rich films. The ensuing increase in film resistance forces the measured potential to higher values in order to maintain the applied current. Once the potential plateau is achieved, negative-going potential transients are observed. No connection was made between the frequency and severity of these events and the applied current. These events are believed to be random, and the success of any individual event relies on the crevice chemistry developed as a consequence of prior events as described earlier. What is apparent is that the average time required for a successful breakdown event to occur, i.e., the incubation time, increases as the applied current decreases. We believe this to be a result of the decreased rate at which the CCS is developed.

Once crevice corrosion is initiated, the propagation potential appears to be independent of the applied current. However, interpretation of crevice behaviour by monitoring changes in the propagation potential is complicated by the large ohmic drop within the active crevice. Once crevice corrosion is initiated, the high solution resistance within the crevice, coupled with the flow of current, results in a potential drop, which means the measured potential is valid only outside the crevice mouth, and not in the crevice interior. Therefore, we have not attempted to understand the behaviour of the propagation potential.

In order to relate features of the measured potential to any corresponding physical damage, we conducted a study in which we withdrew the applied current following characteristic potential behaviour. Of particular interest during this study were the negative-going potential transients occurring during the time of the potential plateau. Knowledge of the early stages of damage allows for more accurate interpretation of fully corroded coupons, which will be discussed later. In total two potential responses were analyzed: that occurring immediately following initiation (Fig. 5A), and that observed after a small amount of propagation had occurred (Fig. 5B).

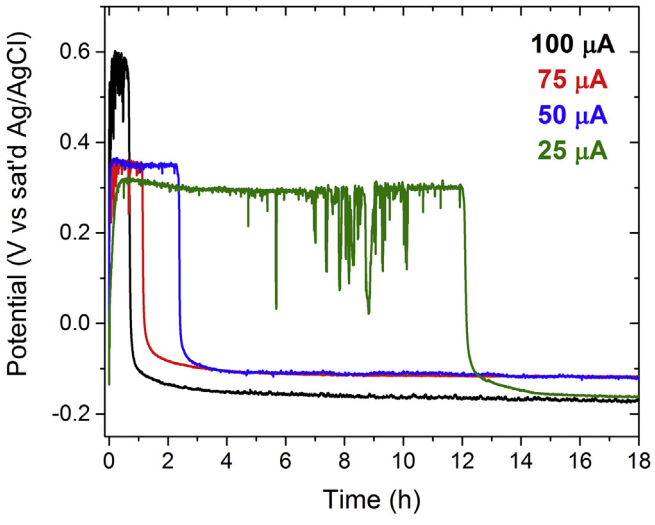

Fig. 4. Potential-time response of C-22 crevice electrode while under galvanostatic control (100, 75, 50, and 25 μA).

As shown in Fig. 5A, immediately following initiation the total amount of damage is minimal, with polishing lines remaining clearly visible. Areas of localized attack are present and appear primarily along grain boundaries. A thin covering of Mo-, W-, and O-rich corrosion products was found surrounding areas of damage. A large amount of these products was detached during the disassembly of the crevice, and it is generally believed that these products deposit to cover areas of damage in acidified crevices [16]. Crevice coupons from experiments that were terminated after a short period of propagation had a similar damage signature; however, damage was intensified, suggesting a natural progression, shown in Fig. 5B. The progression appears to involve predominantly corrosion along grain boundaries. Furthermore, these coupons were again covered by Mo-, W-, and O-rich corrosion products. However, the corrosion product deposits were thicker, as illustrated by the increased EDX signal intensity relative to the background. The deposition of these products has been said to stifle active dissolution, causing active sites to relocate within the crevice [14]. From these experiments we concluded that damage begins at local sites, predominantly along grain boundaries, and progresses as corrosion products begin to deposit.

3.3. Potential behaviour of different alloys

A direct comparison of the potential response observed for BC-1, C-22, and G-30, under the application of 100 μA is outlined in Fig. 6. Upon the application of constant current both BC-1 and C-22 exhibit a rapid increase in potential as a result of oxide growth, as previously discussed. The rate at which the potential increases is dependent on the Cr content of the alloy reflecting the rate of film growth. As a consequence, the potential response of C-22 (22% Cr) increases more rapidly and to a higher final potential than for BC-1 (13% Cr). Furthermore, the frequency and amplitude of breakdown events appears to have a dependence on Mo content. In comparison, BC-1 (22% Mo) displays less frequent potential transients with smaller excursions than C-22 (13% Mo). This is the result of the greater ability of BC-1 to repassivate film breakdown events resulting from increased Mo content. These observations have similarities to those previously discussed in studies employing the galvanostatic crevice corrosion technique on different Ni-Cr-Mo alloys [9].

The potential behaviour seen for alloy G-30 deviates from the previously described behaviour. Although an initial increase in potential is observed, it is short lived and precedes a period of instability followed by successful breakdown. The maximum potential reached is much lower than the threshold potential once thought to be a requirement for the initiation of galvanostatically controlled crevice corrosion of Ni-Cr-Mo alloys [10]. These results, together with a series of additional experiments (not discussed here), suggest differences in oxide film stability in solutions anticipated during the development of crevice corrosion. This could be a result of Mo content insufficient to stabilize the oxide film as acidity develops [2,3]. The cause of this deviation will be the focus of a future publication. Herein, the focus will be on the presence and extent of an internal cathodic reaction as well as the effect of composition on these processes.

In all cases, following a successful initiation event, the propagation potential was found to be relatively stable, aside from only minor fluctuations. Such fluctuations suggest localized breakdown events within the active crevice. Since the final damage

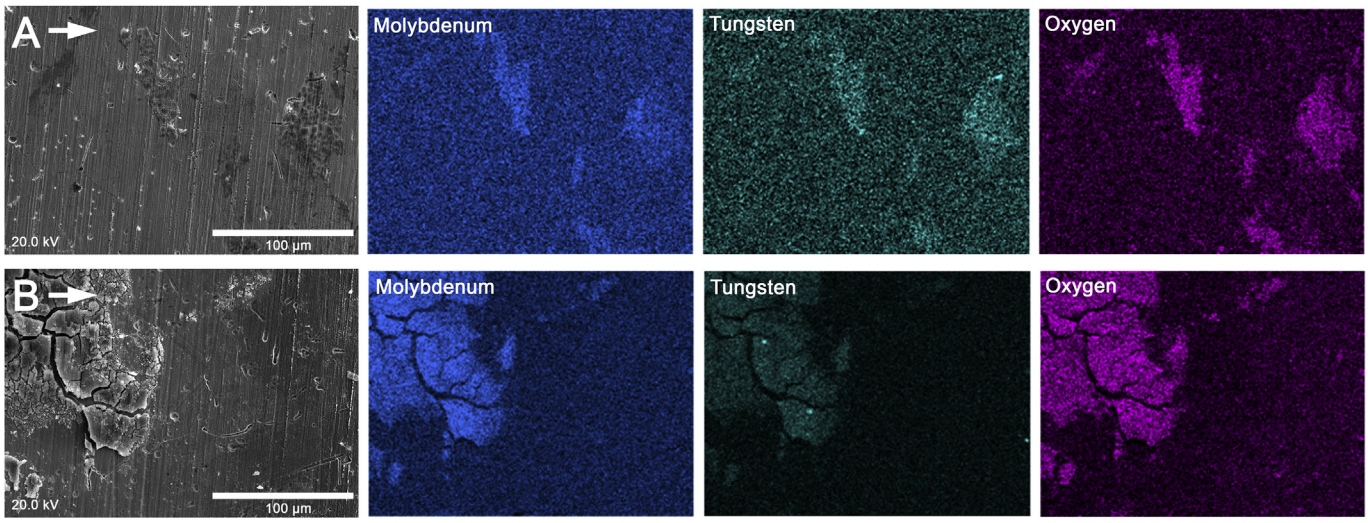

Fig. 5. Secondary electron micrographs and element distribution maps of crevice site following (A) several initiation attempts and (B) successful initiation. Both coupons were corroded galvanostatically at 75 µA.

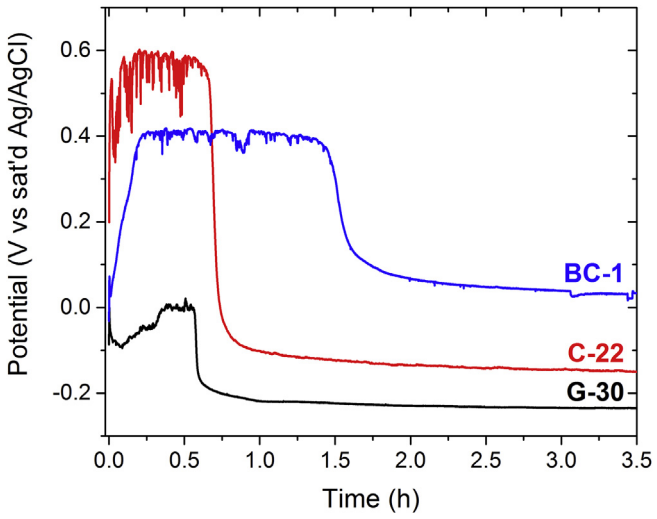

Fig. 6. Comparison of the potential-time response of BC-1, C-22, and G-30, while under galvanostatic control at 100 µA.

morphology displays a single corroded region, it is likely that these potential fluctuations are the result of breakdown events along the periphery of the active crevice. Notably, the propagation potentials were found to decrease as the Mo content of the alloy decreases. This is consistent with previous observations made on different Ni-Cr-Mo alloys [9].

In consideration of each of the propagation potentials, H^+ reduction within the crevice, serving as the additional cathodic reaction, is considered thermodynamically possible. For instance, if the pH inside the active crevice is assumed to be 0, the potential for H^+ reduction at 120 °C is calculated to be 0.035 V (vs sat'd Ag/AgCl) (assuming 1×10^{-6} atm H_2). Since each of the propagation potentials is consistently less than 0.035 V (vs sat'd Ag/AgCl), the H^+ reduction reaction can be considered thermodynamically possible within an active crevice. In addition, the effects of IR drop at locations deep within the creviced region are not accounted for, but would only strengthen the thermodynamic argument. Lastly, the crevice pH used to calculate the reduction potential is conservative, given literature reports that the pH would be < 0 [12,16,17].

3.4. Internal cathodic support

Following the completion of each experiment, crevice coupons were thoroughly cleaned to remove corrosion products formed in damaged areas. With the purpose of obtaining measurable weight loss, each experiment was conducted until a total applied charge (Q_A) of 100 C was reached. The large weight loss which resulted allowed for the accurate calculation of a charge equivalent to the weight loss (Q_W). This was calculated according to Faraday's law, equation (1), where W is the weight loss, F is Faraday's constant, n is the weighted average oxidation number of metal cations created, and M is the effective molar mass, calculated based on the alloy composition.

$$Q_W = WF\left(\frac{n}{M}\right) \tag{1}$$

$$\left(\frac{n}{M}\right) = \sum_{i=1}\left(\frac{f_i n_i}{M_i}\right) \tag{2}$$

The calculation used for the effective oxidation number:molar mass ratio is outlined in equation (2), were f_i is the mass fraction, n_i is the number of electrons transferred during oxidation, and M_i is the molar mass of the respective alloying element. For simplicity, only major alloying elements (Ni, Cr, Mo, W, and Fe) were considered in these calculations and congruent metal dissolution was assumed. Values of f_i were calculated from the nominal compositions reported by Haynes International (Table 1). The values used for n_i were discerned using thermodynamic values for all elements except Mo and W. Based on thermodynamic data, Ni, Cr, and Fe were anticipated to oxidize to form Ni(II), Cr(III), and Fe(II) species in the CCS. The same set of E-pH diagrams indicates the oxidation of Mo and W to Mo(IV) and W(IV) species [16,18]; however, literature reports suggest that the corrosion products formed within an active crevice environment contain mainly Mo(VI) and W(VI) species [13,14]. Furthermore, the calculated effective oxidation number:-molar mass ratio (n/M) is similar to that of other literature reports [19].

In order to determine the extent of internal cathodic support, the total sustained damage (Q_W) was compared to that measured electrochemically (Q_A). The value of Q_A accounts only for the damage sustained by coupling of corrosion to the external

reduction of O_2 on the counter electrode. In contrast, the value of Q_W corresponds to the total amount of damage resulting from corrosion coupled to all possible cathodic reactions. Therefore, the difference between the two values indicates the amount of damage arising from coupling to cathodic reactions occurring within the crevice, i.e., H^+ reduction in the crevice interior. Since negative-going potential transients, observed during the early stages of polarization on all alloys, correspond to localized corrosion events within the crevice, the total Q_A (100 C) was considered rather than only the charge passed after initiation. The extent of internal cathodic support for corrosion of alloy C-22 at a series of applied currents, reported as a percentage of the total amount of corrosion damage (i.e. $\frac{(Q_W - Q_A)}{Q_W} \times 100\%$) is illustrated in Fig. 7. Through this methodology, the presence of an internal cathodic support process is apparent. From these results, it is clear that corrosion rate calculations that consider O_2 as the only oxidant underestimate the extent of corrosion damage.

At the lowest examined current, 25 μA, the contribution of internal cathodic support was significant, but the actual extent of it is irreproducible. The values range, from 22.1 to 45.8%, likely a result of the evolution of damage morphology occurring within the active crevice. Based on post-corrosion analyses, it is apparent that the tendency under the application of small currents is to drive deeper penetration within the crevice. We believe that these deep areas have an increased ability to support the development and/or maintenance of the CCS. Conversely, at higher applied currents, the tendency of damage to spread laterally across an alloy surface is less effective at supporting the developing CCS. The propensity of damage to spread laterally at higher applied current has been discussed elsewhere [14]. The hypothesis that damage morphology plays a role in establishing an internal cathodic reaction will be explored further at the end of this paper.

With the realization that an internal cathodic reaction is indeed significant during the crevice corrosion of C-22 the question remains how the composition of the alloy affects this process. The ability of Mo-rich corrosion products to stifle active dissolution has been investigated in the context of different forms of localized corrosion. In a study focused on artificial pits, Newman showed the tendency of Mo to locate at defect sites, inhibiting dissolution at locations which would otherwise corrode [20,21]. Shan et al. demonstrated the tendency of dissolved Mo and W to precipitate within an active crevice, while other dissolved alloying elements tend to deposit outside the active region [16]. Jakupi et al. later characterized the Mo-rich corrosion products found within an active crevice as polymeric Mo(VI) species using Raman spectroscopy [22]. In the present work, we attempt to characterize the effect of Mo(VI) deposition on internal cathodic support of crevice corrosion by studying the behaviour of Ni alloys G-30, C-22, and BC-1 polarized galvanostatically at a single applied current.

The degree of internal cathodic support determined from $\frac{(Q_W - Q_A)}{Q_W} \times 100\%$ analyses of BC-1, C-22, and G-30 crevice coupons corroded at an applied current of 100 μA are shown in Fig. 8. In this representation, the internal cathodic support is compared to the Mo + W content of the alloy. The two are considered in sum because W behaves much like Mo; i.e., W-rich corrosion products deposit and stifle dissolution [16,23]. This treatment assumes that the magnitude of the effect is the same per unit mass for both Mo and W, however some literature reports claim that Mo is twice as effective as W in protecting an alloy on a per-weight basis [3,24,25]. Whether or not the relative amounts of internal cathodic support in Fig. 8 are compared to the Mo, Mo + 0.5 W, or Mo + W content of each alloy, the conclusions are the same.

The Mo + W content is inversely proportional to the magnitude of the internal support process. As the Mo + W content increases, the extent to which the internal H^+ reduction reaction is able to intensify damage decreases. For alloy G-30, containing only 5.5% Mo and 2.5% W, the internal cathodic reaction has been shown to intensify damage as much as an additional 79.2%. Alloy C-22, which contains 13% Mo and 3% W, has an average 23.8% increase in the expected damage based on the applied charge, while BC-1 (22% Mo) exhibits a weight loss measurement suggesting negligible internal support (approximately zero).

It should be explicitly mentioned that the weight loss method used to quantify the internal support is a rather crude process that relies on removal of the corrosion product, which is difficult, due to the irregular surface morphology and locations of deep penetration. Consequently, the weight loss values used to calculate Q_W represent an underestimate of the actual extent of corrosion damage, and therefore so are the levels of internal cathodic support determined by comparison of Q_A and Q_W. Nonetheless, the data presented highlight the importance of considering such a process, and the extent to which alloy composition may promote or

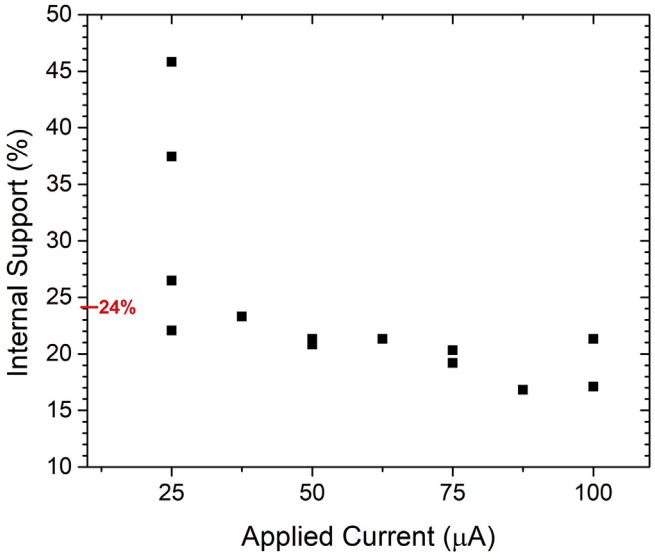

Fig. 7. Internal support (%) as a function of applied current on C-22.

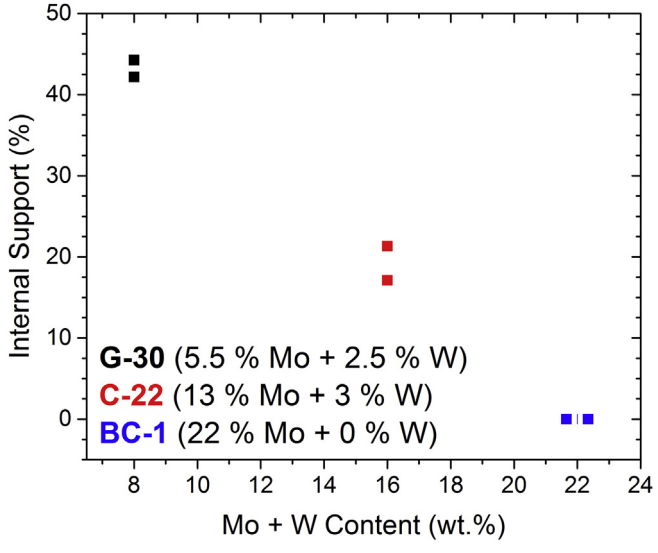

Fig. 8. Internal support (%) as a function of Mo + W content. Coupons corroded galvanostatically at 100 μA.

suppress it.

To support this analysis, an identical experiment (100 C of charge applied at 100 μA) was performed on an alloy G-30 coupon with no crevice. In this case, the potential remained in the transpassive range (~0.82 V (vs sat'd Ag/AgCl)) throughout the entire polarization period, and no negative-going transients were observed. The measured weight loss corresponded to 65.0 C of charge equivalent (compared with 179.2 C for the electrode with the crevice). With no crevice, the weight loss is *less* than expected, rather than more. The "missing" 35 C charge equivalent to weight loss in this experiment likely corresponds to the mass of residual oxide that could not be stripped from the metal surface after the polarization experiment, consistent with the contention that the Q_W values represent an underestimate of the actual extent of corrosion damage.

3.5. Damage progression

The removal of corrosion product from coupons initially used to quantify internal cathodic support also benefitted post-corrosion analyses by exposing the otherwise hidden variations in crevice corrosion damage. Each of the examined alloys illustrates differences in damage morphology, while sharing subtle features, such as those discussed during the study of initiation (Fig. 9). The corrosion damage (Fig. 9A-C) achieved maximum penetration depth in proximity to the crevice mouth. This is a feature commonly observed during the crevice corrosion of Ni-Cr-Mo alloys, and in a practical sense represents and arises from the re-tracing of the active-passive polarization curve within the crevice as a consequence of the local ohmic drop within the occluded geometry [26,27].

In general, the maximum depth of penetration was greatest for alloy G-30. In contrast, alloy BC-1 consistently revealed the lowest maximum depth of penetration. For the damage sites represented in Fig. 9A-C the maximum depth of penetration was found to be approximately 310, 265, and 76 μm on alloys G-30, C-22, and BC-1, respectively.

Information regarding how damage develops within the active crevice was uncovered by comparing the SEM images shown in Fig. 9D-F. Alloy BC-1 (Fig. 9D), shows features which resemble the damage observed during initiation studies (recall Fig. 5). This implies that for this alloy, following initiation, the readily deposited corrosion products impede damage progression and instead force dissolution to relocate along the periphery of the damage site. As a result, the damage morphology fails to develop beyond the features observed during early propagation. This is consistent with the observation that BC-1 typically shows shallow corrosion penetration in comparison to C-22 and G-30. Alloy C-22 (Fig. 9E), which is anticipated to deposit corrosion products less readily, due to the decreased Mo content, shows similar features along the periphery of the crevice, yet has what appears to be a more advanced level of damage in the center of the crevice. This suggests that C-22 requires a longer time to deposit corrosion products sufficient to force the applied current elsewhere (i.e., to the periphery). Lastly, G-30 (Fig. 9F), which is anticipated to have the poorest ability to deposit corrosion products, shows almost no lateral progression of damage.

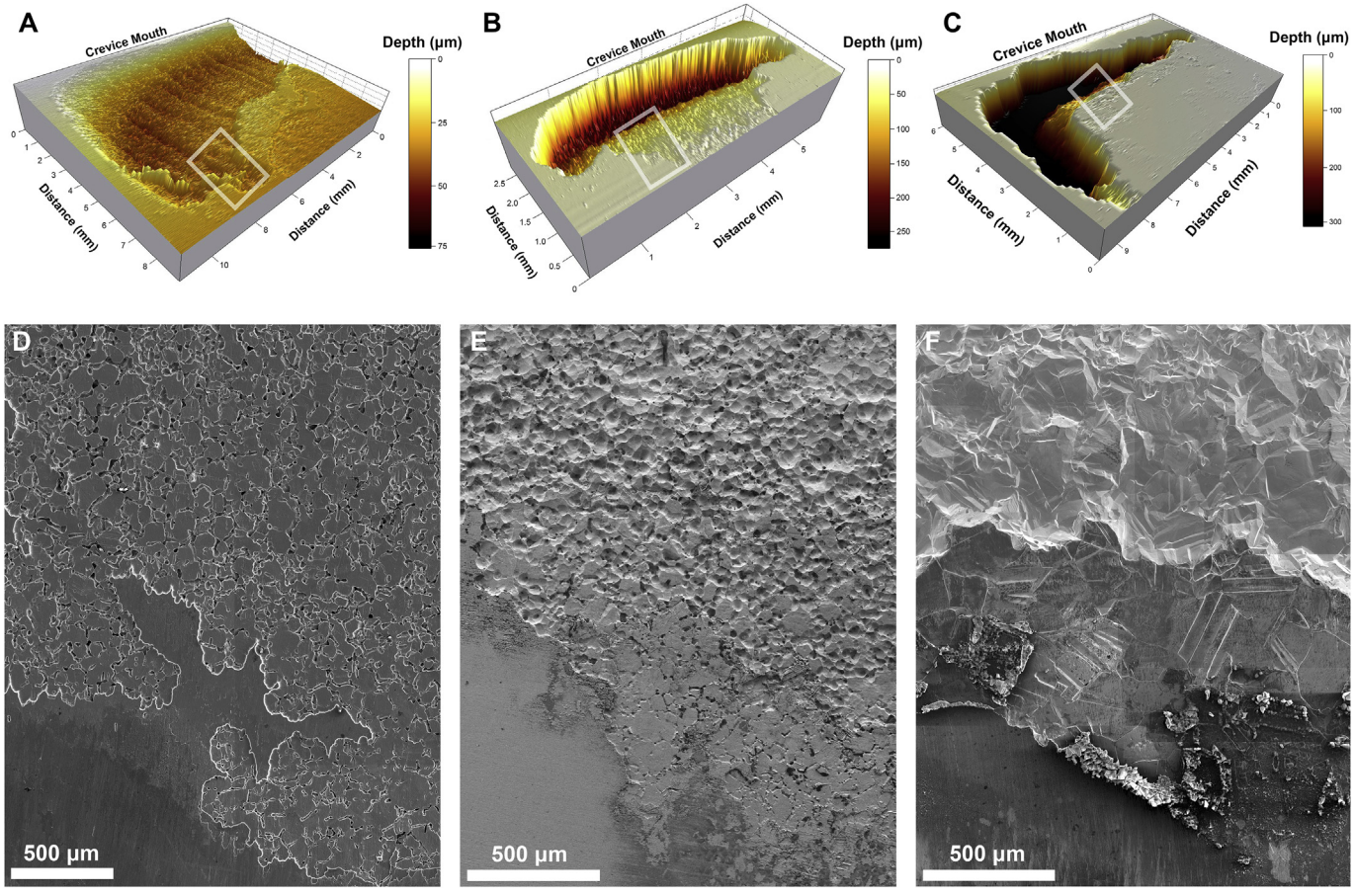

Fig. 9. Three-dimensional reconstruction from surface profilometry (A–C) and secondary electron micrographs (D–F) of crevice damage on BC-1, C-22, and G-30 respectively. Approximate location of each micrograph is indicated on the respective surface profile. All coupons were corroded galvanostatically at 100 μA for a total applied charge of 100 C.

Instead the periphery of the damaged region shows some localized attack along grain boundaries, and displays features of preferential etching. This suggests a global instability of the oxide film exposed to the developing CCS, consistent with observations made during the discussion of the potential response for G-30 under galvanostatic conditions. As one traverses from the periphery toward the area of greatest depth, there is an immediate drop off in topography (shown in both C and F) which suggests the failure of Mo-rich products to deposit on the surface. This is consistent with literature reports which have shown that an increased rate of molybdate deposition forces damage to spread laterally across the surface [14]. The ineffective deposition process occurring on G-30 allows active metal dissolution to continue relatively uninhibited, and therefore damage penetrates deep into the bulk material.

Conclusions may be drawn between changes in crevice geometry and the intensity of the internal H^+ reduction reaction. Greater crevice corrosion penetration depths, whether the result of low Mo (and W) content or low applied current (discussed above), coincide with a higher degree of internal cathodic support. Based on our observations, internal cathodic support of crevice corrosion is less important on alloys containing high amounts of Mo (and W). It appears that these alloys develop a crevice geometry that is less suitable for the development of the CCS, and that the deposition of Mo- and W-rich corrosion products limits the surface area available for the H^+ reduction reaction within the crevice. At low applied currents, damage is limited to a small area and penetrates deep into the alloy surface, and conversely, when high currents are applied, the corrosion reaction and the consequent damage are forced to spread laterally across the surface. This suggests that a key factor in the crevice corrosion process may be the maintenance of a minimum local current density at active sites. This suggests that under natural (vs galvanostatically-driven) corrosion conditions, crevice corrosion damage will tend to penetrate deeply in limited areas, rather than spreading laterally across the surface. Therefore, the susceptibility of an alloy to enhancement of crevice corrosion by coupling to the internal cathodic reaction seems to be determined by the content of Mo + W, which hinder internal H^+ reduction by blocking the potentially cathodic surface with corrosion products and by limiting the establishment of a crevice geometry conducive to development of the CCS.

The hypothesis of corrosion product deposition governing the damage morphology and internal cathodic support is reinforced by the fact that the metallographic features of each alloy are similar; hence, there are no obvious microstructural features that could contribute to the differences in damage morphology between alloys. Previously published work has demonstrated that the corrosion susceptibility of the grain boundaries within a Ni-Cr-Mo alloy depends to some degree on their coincidence site lattice (CSL) classification (Σ value) [28,29]. Of particular interest are the Σ3 and the Σ(>29) boundaries, the latter being termed random boundaries (R). These boundaries are considered low- and high-energy, respectively. The random boundaries have been shown to be more susceptible to attack than the lower energy boundaries [10,28,30].

We used EBSD to quantify the abundance on the three alloys of grain boundaries of each CSL Σ value. The results are presented in Fig. 10. We found no significant difference in grain boundary make-up between the alloys; each alloy contains approximately 70% Σ3 boundaries. This is explained by the face-centred-cubic lattice and the similar heat treatment imposed on the alloys during fabrication. Given that each alloy possesses approximately the same abundance of random grain boundaries, which are particularly susceptible to corrosion, one might expect the damage to follow similar progression for each alloy, however, the results shown in Fig. 9 demonstrate otherwise. Therefore, the differences in damage

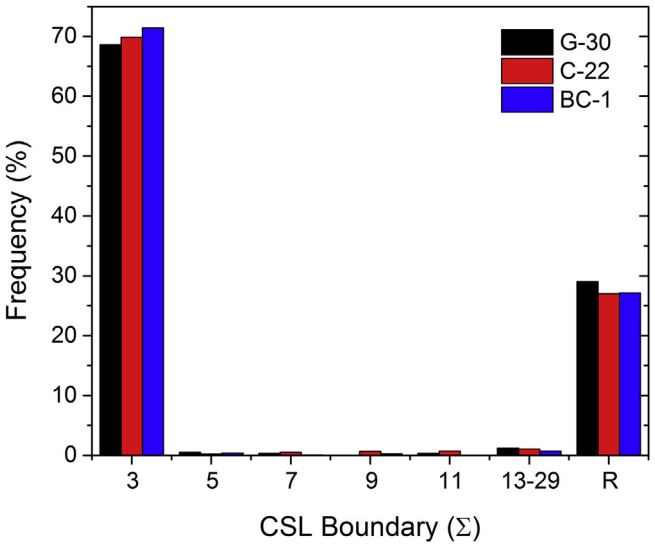

Fig. 10. Frequency of ordered grain boundaries according to coincidence site lattice notation for Hastelloy G-30, C-22, and BC-1. Random grain boundaries (R) are defined as Σ(>29).

morphology between alloys must be the result of differences in composition. Likewise, there is no apparent microstructural feature that would render one alloy more or less susceptible to the intergranular attack discussed above. Instead, it is likely that changes occurring within the occluded region (i.e., deposition of corrosion products) control the evolution of damage morphology. On alloy BC-1, which has the highest Mo + W content, the damage never gets beyond the initial stages and instead is forced to spread laterally across the surface. Alloy C-22, which has a moderate Mo + W content, has areas surrounding the central damage site which resemble early stages of corrosion. However, in the central areas the damage is more developed and crevice corrosion begins to attack grain bodies indiscriminately. On alloy G-30, which has the lowest Mo + W content, crevice corrosion damage penetrates deeply, possibly providing a more optimum environment to sustain the internal H^+ reduction reaction.

4. Conclusions

The presence of an internal cathodic support reaction, likely H^+ reduction, occurring during the crevice corrosion of Ni-based alloys has been implicitly demonstrated. For the investigated alloys, this process has been found to have the ability to intensify the anticipated crevice damage by as much as ~79%. The intensity of H^+ reduction within the crevice is thought to be dependent on the evolving geometry of the host crevice and the blocking of cathodic sites by deposition of Mo- and W-rich corrosion products. Crevice damage that penetrates deeply supports the development of the CCS, and therefore the internal H^+ reduction reaction. As a result, low-Mo and W alloys, such as alloy G-30, are particularly susceptible to this process. Consequently, we conclude that Mo- and W-rich corrosion products not only stifle active dissolution, but also limit the ability of H^+ reduction to intensify damage.

Furthermore, damage was also found to penetrate more deeply when the alloys were driven to corrode by small applied currents than when large currents were applied. This is particularly concerning for corrosion under natural conditions, where the applied current is zero.

Finally, our work demonstrates that corrosion damage predictions based solely on the availability of O_2 and other oxidants in

the service environment will significantly underestimate the actual extent of corrosion on Ni-based alloys, an important concern that has not previously been demonstrated.

Acknowledgements

The authors wish to thank Surface Science Western, especially Mr. Brad Kobe and Dr. Heng-Yong Nie, for their crucial assistance with operation of surface analytical equipment. We thank NSERC and Haynes International for supplying research funding and for the donation of materials, respectively. Author J.D.H. is also grateful to be the recipient of an NSERC CGS-D scholarship.

References

[1] K. Hashimoto, K. Asami, A. Kawashima, H. Habazaki, E. Akiyama, The role of corrosion-resistant alloying elements in passivity, Corrosion Sci. 49 (2007) 42–52.
[2] V. Maurice, H. Peng, L.H. Klein, A. Seyeux, S. Zanna, P. Marcus, Effects of molybdenum on the composition and nanoscale morphology of passivated austenitic stainless steel surfaces, Faraday Discuss 180 (2015) 151–170.
[3] A. Mishra, D.W. Shoesmith, P. Manning, Materials selection for use in concentrated hydrochloric acid, Corrosion 73 (2017) 68–76.
[4] J.W. Oldfield, W.H. Sutton, Crevice corrosion of stainless steels II, Exp. Stud. Br. Corrosion J. 13 (1978) 104–111.
[5] J.W. Oldfield, W.H. Sutton, Crevice corrosion of stainless steels I. A mathematical model, Br. Corrosion J. 13 (1978) 13–22.
[6] J.J. Noël, The Electrochemistry of Titanium Corrosion, PhD Thesis, Department of Chemistry, University of Manitoba, Winnipeg, Manitoba, 1999.
[7] X. He, J.J. Noël, D.W. Shoesmith, Temperature dependence of crevice corrosion initiation on titanium grade-2, J. Electochem. Soc. 149 (2002) B440–B449.
[8] L. Yan, J.J. Noël, D.W. Shoesmith, Hydrogen absorption into Grade-2 titanium during crevice corrosion, Electrochim. Acta 56 (2011) 1810–1822.
[9] N. Ebrahimi, P. Jakupi, J.J. Noël, D.W. Shoesmith, The role of alloying elements on the crevice corrosion behavior of Ni-Cr-Mo alloys, Corrosion 71 (2015) 1441–1451.
[10] N. Ebrahimi, J.J. Noël, M.A. Rodriguez, D.W. Shoesmith, The self-sustaining propagation of crevice corrosion on the hybrid BC1 Ni–Cr–Mo alloy in hot saline solutions, Corrosion Sci. 105 (2016) 58–67.
[11] P. Marcus, On some fundamental factors in the effect of alloying elements on passivation of alloys, Corrosion Sci. 36 (1994) 2155–2158.
[12] N.S. Zadorozne, C.M. Giordano, M.A. Rodriguez, R.M. Carranza, R.B. Rebak, Crevice corrosion kinetics of nickel alloys bearing chromium and molybdenum, Electrochim. Acta 76 (2012) 94–101.
[13] P. Jakupi, J.J. Noël, D.W. Shoesmith, Crevice corrosion initiation and propagation on Alloy-22 under galvanically-coupled and galvanostatic conditions, Corrosion Sci. 53 (2011) 3122–3130.
[14] P. Jakupi, J.J. Noël, D.W. Shoesmith, The evolution of crevice corrosion damage on the Ni–Cr–Mo–W alloy-22 determined by confocal laser scanning microscopy, Corrosion Sci. 54 (2012) 260–269.
[15] P. Jakupi, D. Zagidulin, J.J. Noël, D.W. Shoesmith, Crevice corrosion of Ni-Cr-Mo alloys, ECS Trans. 3 (2007) 259–271.
[16] X. Shan, J.H. Payer, Characterization of the corrosion products of crevice corroded alloy 22, J. Electochem. Soc. 156 (2009) C313–C321.
[17] M. Nishimoto, J. Ogawa, I. Muto, Y. Sugawara, N. Hara, Simultaneous visualization of pH and Cl– distributions inside the crevice of stainless steel, Corrosion Sci. 106 (2016) 298–302.
[18] R.S. Lillard, M.P. Jurinski, J.R. Scully, Crevice corrosion of alloy 625 in chlorinated ASTM artificial ocean water, Corrosion Sci. 50 (1994) 251–265.
[19] J.R. Hayes, J.J. Gray, A.W. Szmodis, C.A. Orme, Influence of chromium and molybdenum on the corrosion of nickel-based alloys, Corrosion Sci. 62 (2006) 491–500.
[20] R. Newman, The dissolution and passivation kinetics of stainless alloys containing molybdenum (part II), Corrosion Sci. 25 (1985) 341–350.
[21] R. Newman, The dissolution and passivation kinetics of stainless alloys containing molybdenum (part I), Corrosion Sci. 25 (1985) 331–339.
[22] P. Jakupi, F. Wang, J.J. Noël, D.W. Shoesmith, Corrosion product analysis on crevice corroded Alloy-22 specimens, Corrosion Sci. 53 (2011) 1670–1679.
[23] M. Miyagusuku, R.M. Carranza, R.B. Rebak, Inhibition mechnaism of phosphate ions on chloride-induced crevice corrosion of alloy 22, Corrosion 71 (2015) 574–584.
[24] E.C. Hornus, C.M. Giordano, M.A. Rodriguez, R.M. Carranza, R.B. Rebak, Effect of temperature on the crevice corrosion of nickel alloys containing chromium and molybdenum, J. Electochem. Soc. 162 (2015) C105–C113.
[25] E.C. Hornus, M.A. Rodriguez, R.M. Carranza, C.M. Giordano, R.B. Rebak, Effect of environmental variables on crevice corrosion susceptibility of Ni-Cr-Mo alloys for nuclear repositories, Proced. Mater. Sci. 8 (2015) 11–20.
[26] G.F. Kennell, R.W. Evitts, Crevice corrosion cathodic reactions and crevice scaling laws, Electrochim. Acta 54 (2009) 4696–4703.
[27] G.F. Kennell, R.W. Evitts, K.L. Heppner, A critical crevice solution and IR drop crevice corrosion model, Corrosion Sci. 50 (2008) 1716–1725.
[28] P. Jakupi, J.J. Noël, D.W. Shoesmith, Intergranular corrosion resistance of Sigma-3 grain boundaries in alloy 22, Electrochem. Solid State Lett. 13 (2010) C1–C3.
[29] N. Ebrahimi, P. Jakupi, A. Korinek, I. Barker, D.E. Moser, D.W. Shoesmith, Sigma and random grain boundaries and their effect on the corrosion of the Ni-Cr-Mo alloy 22, J. Electochem. Soc. 163 (2016) C232–C239.
[30] J.J. Gray, B.S. El Dasher, C.A. Orme, Competitive effects of metal dissolution and passivation modulated by surface structure: an AFM and EBSD study of the corrosion of alloy 22, Surf. Sci. 600 (2006) 2488–2494.